Corrosion Science 59 (2012) 157–168

Contents lists available at SciVerse ScienceDirect

Corrosion Science

journal homepage: www.elsevier.com/locate/corsci

Corrosion resistance and mechanism of steel rebar coated with three types of enamel

Fujian Tang [a], Genda Chen [a,*], Richard K. Brow [b], Jeffery S. Volz [a], Michael L. Koenigstein [c]

[a] Department of Civil, Architectural, and Environmental Engineering, Missouri University of Science and Technology, Rolla, MO 65409-0030, USA
[b] Department of Materials Science and Engineering, Missouri University of Science and Technology, Rolla, MO 65401, USA
[c] Pro-Perma Engineered Coatings, Hypoint, Rolla, MO 65401, USA

ARTICLE INFO

Article history:
Received 7 September 2011
Accepted 28 February 2012
Available online 9 March 2012

Keywords:
A. Steel
A. Ceramic
B. EIS
B. SEM
B. XRD

ABSTRACT

Corrosion resistances of steel rebar with different enamel coatings, and with fusion bonded epoxy coatings were investigated in 3.5 wt.% NaCl solution by Electrochemical Impedance Spectroscopy (EIS). The sensitivity to damage of the coatings was characterized and it was found that the pure and double enamel coatings can protect the steel rebar better than the mixed enamel coating due to their denser microstructures with isolated pores. Damaged enamel coating was locally corroded, whereas corrosion at a defect often undercut the epoxy coating. The intact epoxy coating offered better corrosion protection than the enamel coatings.

Published by Elsevier Ltd.

1. Introduction

Corrosion of reinforcing steel is common in reinforced concrete structures around the world. It causes premature deterioration of civil infrastructures such as highway and railway bridges, offshore platforms, pipelines, and dams. According to Koch et al. [1], the annual cost of corrosion in the United States is approximately $8 billion for highway bridges alone. Corrosion of reinforcing steel in concrete results from two main sources: carbonization and chloride penetration [2]. Chloride mainly comes from road deicing salts in winter for highways and bridges, and marine climate for offshore and coastal structures. One effective way to prevent or slow down the penetration process of these aggressive ions is to apply a coating on the rebar surface that would establish a physical barrier between the steel and concrete.

Ceramic porcelain enamel coatings for steel possess chemical and mechanical stability in various environments including acid, alkaline, high temperature and harsh working conditions [3], and so are widely used for a variety of consumer applications and for the protection of steel in many industrial chemical applications. The degradation mechanism of enamel coated steel has been investigated by several researchers [4,5]. Recently, enamel coated reinforcing steel for pavement and stay-in-place forms have been investigated by researchers with the Army Corps of Engineers [6–8]. They modified standard enamel compositions by adding a reactive phase, like Ca-silicate, that would bond to the surrounding concrete matrix, and concluded that enamel coatings improve the corrosion resistance and enhance the bond strength with surrounding concrete. However, corrosion resistance of different enamel coatings and their tolerance to existing damage have not been studied and quantified systematically. In particular, the concept of a two-layer coating, one to enhance bond strengths and the other to improve corrosion resistance, has never been explored prior to this study.

In this study, corrosion resistances of enamel coated steel rebar were evaluated in 3.5 wt.% NaCl solution by electrochemical impedance spectroscopy (EIS). The enamel coating systems tested include a pure enamel, an enamel mixed with 50% calcium silicate (by weight), and a double enamel with an inner layer of pure enamel and an outer layer of the mixed enamel. Their corrosion performance was compared with commonly used fusion bonded epoxy (FBE) coating in reinforced concrete structures. The phase composition and microstructure of enamel coatings were characterized by X-ray diffraction (XRD) and scanning electron microscopy (SEM) coupled with an energy-dispersive X-ray spectroscopy (EDS). Impact tests were performed on some samples to investigate the effect of coating damage on its corrosion resistance. The barrier ability of enamel coatings to aggressive ions was confirmed by mapping the chloride distribution in the coating of tested rebar.

* Corresponding author. Address: Department of Civil, Architectural, and Environmental Engineering, Missouri University of Science and Technology, 328 Butler-Carlton Hall, 1401 N. Pine Street, Rolla, MO 65409-0030, USA. Tel.: +1 573 341 4462; fax: +1 573 341 4729.
E-mail address: gchen@mst.edu (G. Chen).

0010-938X/$ - see front matter Published by Elsevier Ltd.
http://dx.doi.org/10.1016/j.corsci.2012.02.024

2. Experimental details

2.1. Preparation of enamel coatings

Enamels are typically silicate-based materials that are deposited from slurries and fused at high temperature. The enamel slurry is made by milling glass frits, clay and certain electrolytes, then mixing with water to provide a stable suspension. In this study, a commercially-available alkali borosilicate glass frit from PEMCO (Product No. PO2025) was used for the pure enamel (PE). Its chemical composition is given in Table 1 [9]. This composition was selected because it contains ZrO_2 which is known to improve the durability of glasses exposed to alkaline environments, including cement [10]. A slurry of the pure enamel was made by first adding 454 kg of enamel frit to 189.3 l of water and mixing them for 20 min, and then adding clay (31.8 kg) and borax (2.3 kg) as suspension agents, and mixing again for 3.5 h. The mixed enamel (ME) coatings were prepared by adding 50% (by weight) calcium silicate into pure enamel frits. Calcium silicate particles from the Portland cement specified in ASTM C150-07 [11] were used. Double enamel coating (DE) consists of two layers, the first (inner) layer is a PE coating and the second (outer) is an ME coating.

Commercial steel rebar (12.7 mm diameter) was used in this study. Its chemical composition was determined and is given in Table 2. Before coating, all rebar was sand-blasted and cleaned with commercially available cleansing solvent. For PE and ME coatings, the cleaned rebar was dipped into their corresponding liquid slurry, and heated for 2 min at 150 °C to drive off moisture then fired at 810 °C for 10 min, and finally cooled to room temperature. For the double enamel (DE) coating, the rebar was first dipped into the PE slurry and heated for 2 min at 150 °C to drive off moisture, then dipped into the ME slurry and heated to 150 °C again to drive off moisture, then moved into furnace to fire for 10 min at 810 °C. The firing treatment at high temperature was used to melt the glass frit and chemically bond the enamel to the steel. During enameling, the deformed bar was hung vertically in the furnace; thus, the coating thickness around rebar ribs may not be uniform due to gravity effect.

2.2. Preparation of the samples

The coated steel bars were cut into 89.0 mm lengths with two ends encased in PVC tubes containing epoxy resin. A copper wire was connected electrically at one end of the rebar. The actual length of steel rebar exposed to the corrosive environment was approximately 50.8 mm in the middle portion, as shown in the schematic view of samples in Fig. 1. In addition, commercial FBE coated rebar samples with the same rebar size were also prepared for comparison.

To study the effect of coating damage on the corrosion resistance, some samples were pre-damaged using an impact test apparatus designed according to the ASTM Standard G14 [12]. The apparatus consists of a 0.91 kg steel rod with a hemispherical head, a vertical section of hollow aluminum tubing to guide the rod, and a horizontal section of steel angle to position the coated rebar sample. The coated rebar was secured to the steel angle with clamps, and the weight rod was dropped from a height of 45.7 cm to damage the coatings. Two damage extents were considered, samples with 6 impact points and samples with 12 impact points. Examples of the rebar samples ready for corrosion tests with no coating (UN), with different coatings, and with impact points, are shown in Fig. 2. A total of 39 rebar samples were prepared as detailed in Table 3, taking into account the rebar coating (UN, FBE, PE, ME, and DE) and damage extent (0 = no damage, 1 = 6 impact points, or 2 = 12 impact points). Each sample was designated by a string of letters and numbers. The designation starts with two letters for the type of coating and then two numbers for the number of impact points, which were followed by a # sign and another number representing the number of samples in the same group. The uncoated rebar samples were undamaged and not cleaned prior to corrosion tests, to simulate their as-received condition at a construction site, and so a black oxide layer (mill scale) was initially present on their surfaces.

2.3. Characterization and barrier ability of enamel coatings

The phase composition of three types of enamel coatings and the oxide layer of uncoated rebar before and after corrosion tests were examined directly on the rebar surface with X-ray diffraction (XRD, Philip X' Pert). The microstructure and the elemental analysis of the coatings before corrosion test were investigated by scanning electron microscopy (SEM, Hitachi S4700) coupled with an energy-dispersive X-ray spectroscopy (EDS). At the completion of corrosion tests, the ability of enamel coatings as a barrier to aggressive ions was investigated with SEM by mapping the chloride profile in the enamel coating of rebar. For SEM measurements, one 4.0 mm thick cross-section sample, mounted in epoxy, was cut from each of the coated and uncoated rebar, and then abraded with silicon carbide papers with grits of 80, 180, 320, 600, 800 and 1200. After abrading, all samples were rinsed with deionized water and dried prior to microscopy study.

2.4. Electrochemical studies

All samples were immersed in 3.5 wt.% salt solution consisting of distilled water and purified sodium chloride. Samples were tested at room temperature with a typical three-electrode setup, including a 25.4 mm × 25.4 mm × 0.254 mm platinum sheet as a counter electrode, saturated calomel electrode (SCE) as a reference electrode, and one rebar sample as a working electrode. All three electrodes were connected to a Gamry, Reference 600 potentiostat/galvanostat/ZRA for data acquisition. The electrochemical impedance spectra were obtained with an applied sinusoidal

Table 1
Chemical composition of alkali borosilicate glass frit.

Element	SiO_2	B_2O_3	Na_2O	K_2O	CaO	CaF_2	Al_2O_3	ZrO_2	MnO_2	NiO	CoO
Wt.%	44.0	19.3	15.8	2.8	0.1	4.7	4.6	5.3	1.5	1.0	0.9

Table 2
Chemical composition of steel rebar.

Element	C	Si	Mn	P	S	Cr	Mo	Ni	Co	Cu	V	Sn	Fe
Wt.%	0.383	0.184	1.000	0.115	0.064	0.103	0.069	0.198	0.013	0.373	0.022	0.028	97.40

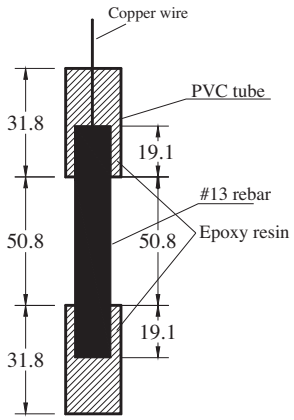

Fig. 1. Geometry of rebar samples (unit: mm).

potential wave of 10 mV amplitude and frequency ranging from 100 kHz to 0.005 Hz at a sampling rate of 5 points per decade.

3. Results and discussion

3.1. Microstructures and elemental analysis

Fig. 3 shows cross-sectional SEM images and representative EDS analyses of uncoated and enamel coated rebar samples. These cross-sections were taken between two ribs, where the coating is relatively uniform and thicker than that over the ribs. EDS analyses were performed on the coating sample taken within the small square in the respective SEM images. The uncoated rebar, Fig. 3a-1, has a thin (about 25 μm thick) oxide layer (mill scale) on the rebar surface, which mainly consists of iron (Fe) and oxygen (O) as shown in Fig. 3a-2. This was likely formed during the hot rolling process of steel production. The pure enamel (PE) coating is approximately 150 μm thick, and has air voids with the maximum diameter of approximately 50 μm, Fig. 3b-1. The air voids result from bubbles that typically form in the molten glass during the high temperature enamel firing process. EDS analysis as shown in Fig. 3b-2 indicates that the principal components in the PE coating include sodium (Na), calcium (Ca), silicon (Si) and aluminum (Al); boron, a major component of the glass frit, could not be detected by the EDS system used. The ME coating is approximately 250 μm thick and it possesses a more complex structure with irregular pore characteristics and relatively high porosity as illustrated in Fig. 3c-1. This porous structure was further verified by the penetration of mounting epoxy during preparation of the SEM sample as shown in Fig. 3c-2. EDS analysis revealed that the ME coating includes a higher content of Ca than the PE coating, Fig. 3c-3, which is consistent with the addition of calcium silicate. The EDS spectrum from the ME coating also exhibited a significant peak of iron (Fe) that presumably originates from the rebar substrate during the chemical reaction at firing temperature. Fig. 3d-1 shows an SEM image of the DE coating. It clearly indicates the presence of two distinct layers, approximately 160 and 240 μm thick for the inner and outer layers, respectively. The inner pure enamel layer exhibits the same microstructure of trapped air voids as found in the PE sample in Fig. 3b-1. Its EDS spectrum, Fig. 3d-2, is consistent with the components of enamel glass with a small peak of iron (Fe) from the rebar substrate. The outer 50/50 enamel layer has a slightly different microstructure from the ME sample in that less mounting epoxy was found to have penetrated through the outer layer. This is likely because, during the second firing process, some of the inner melted pure enamel flowed towards the outer 50/50 enamel, and partially filled and isolated what would otherwise be connected pores in the outer layer as observed in the ME coating, Fig. 3c-1. Even though the pores in outer layer of the DE sample become disconnected, the EDS spectrum of the outer layer is similar to the ME sample, Fig. 3d-3, except that no iron (Fe) was detected since the outer layer was separated from the steel substrate by the inner layer.

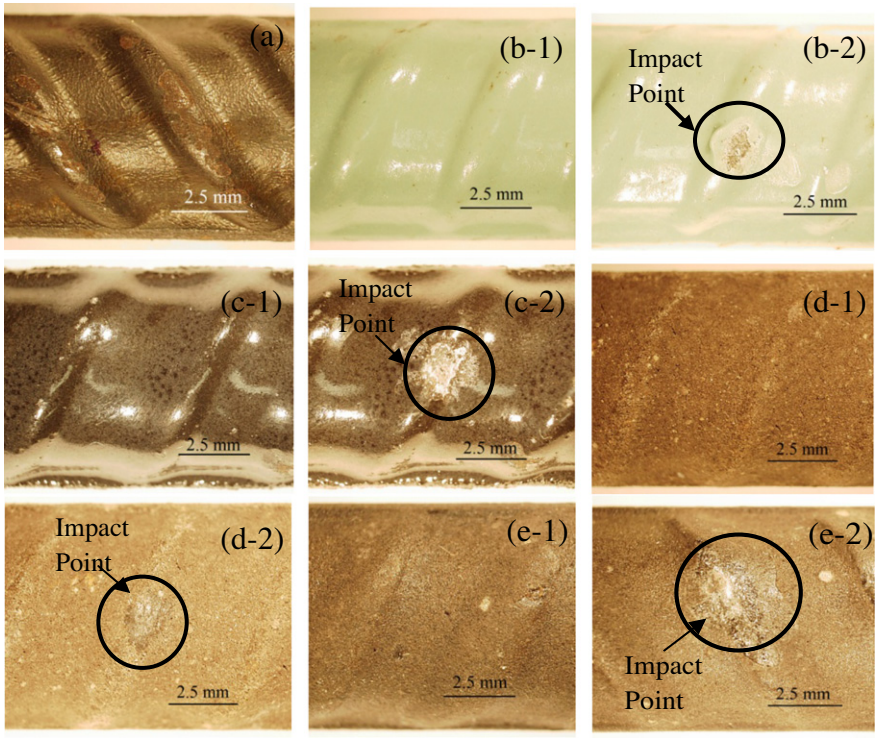

Fig. 2. Steel rebar samples tested in this study: (a) uncoated rebar, (b-1, b-2) FBE coated rebar without and with impact points, (c-1, c-2) pure enamel coated rebar without and with impact points, (d-1, d-2) mixed enamel coated rebar without and with impact points, and (e-1, e-2) double enamel coated rebar without and with impact points.

Table 3
Test matrix: 39 samples total.

Surface condition	Numbers of impact point		
	0	6	12
FBE coating	EP00#1 EP00#2 EP00#3	EP01#1 EP01#2 EP01#3	EP02#1 EP02#2 EP02#3
Pure enamel	PE00#1 PE00#2 PE00#3	PE01#1 PE01#2 PE01#3	PE02#1 PE02#2 PE02#3
Mixed enamel	ME00#1 ME00#2 ME00#3	ME01#1 ME01#2 ME01#3	ME02#1 ME02#2 ME02#3
Double enamel	DE00#1 DE00#2 DE00#3	DE01#1 DE01#2 DE01#3	DE02#1 DE02#2 DE02#3
Uncoated	UN00#1 UN00#2 UN00#3	–	–

Note: Sample ME00#3 was damaged before testing and thus no data is reported in this paper.

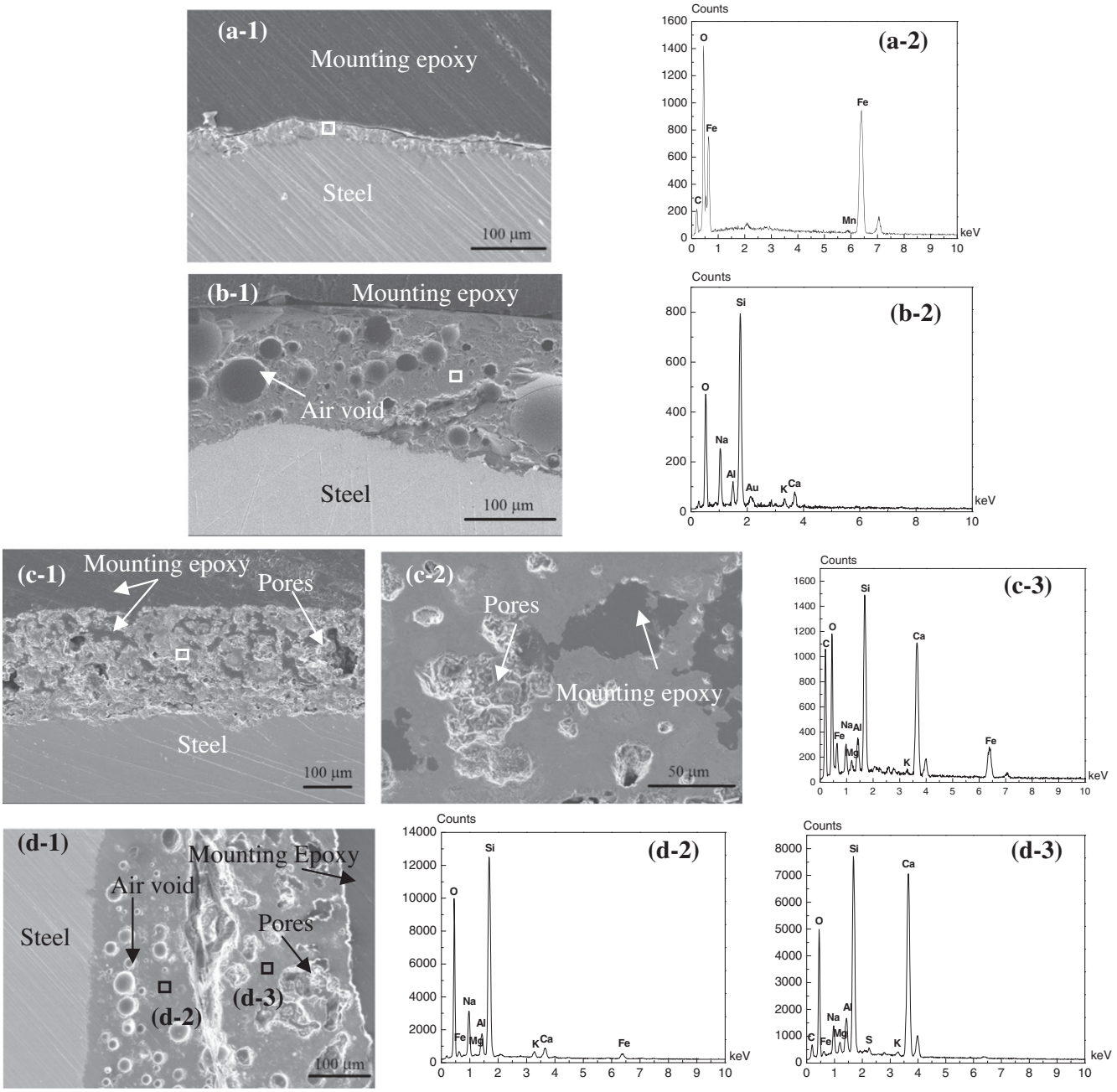

Fig. 3. Cross-sectional SEM images and EDS analysis before corrosion tests: (a-1, a-2) uncoated rebar, (b-1, b-2) pure enamel coated rebar, (c-1, c-2, c-3) mixed enamel coated rebar, and (d-1, d-2, d-3) double enamel coated rebar.

3.2. Coating analysis

Fig. 4 shows the X-ray diffraction analyses on the surface of the uncoated and three enamel coated rebar samples prior to and after corrosion tests immersed in 3.5 wt.% NaCl solution. Magnetite (Fe_3O_4) and Maghemite (Fe_2O_3) are the two main oxides on the uncoated steel rebar surface prior to the corrosion test, consistent with reports on the nature of the mill scale on rebar [13,14]. After

the corrosion test, one rust layer was formed and mainly consisted of lepidocrocite (γ-FeOOH) and akaganeite (β-FeOOH) as shown in Fig. 4a-2 [15–17]. As shown in Fig. 4b-1, some crystalline quartz (SiO_2), could be detected in an otherwise amorphous PE coating. A similar distribution of phases was found on the PE coating after the immersion test, Fig. 4b-2. The presence of some sodium chloride (NaCl) on this latter sample is attributed to the salt solution in which the sample was immersed. Crystalline Ca-silicate phases were detected in both the ME and DE coatings. These phases are present in the Portland cement added to the pure enamel slurry used to produce the ME coating prior to corrosion tests, as shown in Fig. 4c-1 and d-1. After corrosion tests, no change in main components was observed for the DE coating. However, some lepidocrocite (γ-FeOOH) was observed in the ME coating, which is attributed to the corrosion that occurred in the immersion test.

3.3. Electrochemical study

3.3.1. FBE coated steel bar

Fig. 5 presents the electrochemical impedance spectra of the FBE coated rebar samples immersed in 3.5 wt.% NaCl solution. Specifically, the modulus and the phase angle of the complex impedance, Z, for intact and damaged samples are plotted as a function of frequency in Fig. 5a and b, respectively. It can be seen from Fig. 5 that the intact FBE coating displayed capacitive behavior since the modulus-frequency curve is a 45° straight line and the phase angle fluctuates around −90°. Therefore, the intact FBE coating is an effective corrosion barrier for steel rebar. However, damaged FBE coating behaved quite differently. The impedance magnitude was significantly reduced from 10^6 to 0.1 MΩ cm^2 at 0.005 Hz, and the phase-frequency plot can be characterized with two time constants. The first time constant at low frequencies was attributed to the resistance and capacitance of the steel-electrolyte interface, the second time constant at high frequencies was due to the resistance and capacitance of the FBE coating. The significant change in the impedance spectra was caused by impact-induced damage that provided a pathway for chloride ions to penetrate through and resulted in corrosion of the coated rebar in the NaCl solution. No significant difference in corrosion performance was observed between the FBE coated rebar with 6 impact points and with 12 impact points. These findings are in reasonable agreement with previous studies on intact and defective paint systems [18,19].

The electrical equivalent circuit (EEC) as shown in Fig. 6a was used to model the corrosion system with intact FBE coated rebar. Here, R_s represents the solution resistance between the reference electrode and the samples, C_{dl} and R_{ct} represent the double layer capacitance and the charge transfer resistance at the interface between the epoxy coating and the substrate steel. For damaged FBE coating, a different EEC model as shown in Fig. 6b was used to fit the EIS test results. This EEC model is widely used for the evaluation of coating performance and electrochemical behavior of reinforcing steel in concrete [20–23]. The EEC model consists of the solution resistance (R_s), the resistance and capacitance (R_c and CPE_c) of FBE coating, and the charge transfer resistance and double layer capacitance (R_{ct} and CPE_{dl}) of the interface between electrolyte solution and substrate steel. Replacement of the capacitance C for the intact FBE coated rebar in Fig. 6a with the constant phase element (CPE) in Fig. 6b was attributed to the non-homogeneity induced by the coating damage [24–27]. CPE is defined by two parameters Y and n. When $n = 1$, CPE resembles a capacitor with capacitance Y. When $n = 0$, CPE represents a resistor with resistance Y^{-1}. The effective capacitance was calculated according to the following equation [28]:

$$C = Y^{\frac{1}{n}} R^{\frac{1-n}{n}} \tag{1}$$

where R is referred to R_c and R_{ct} when the coating capacitance C_c and the double layer capacitance C_{dl} are calculated, respectively. Correspondingly, CPE_c is represented by Y_c and n_c, and CPE_{dl} by Y_{dl} and n_{dl}. ZSimpWin software was used to fit the EEC model into

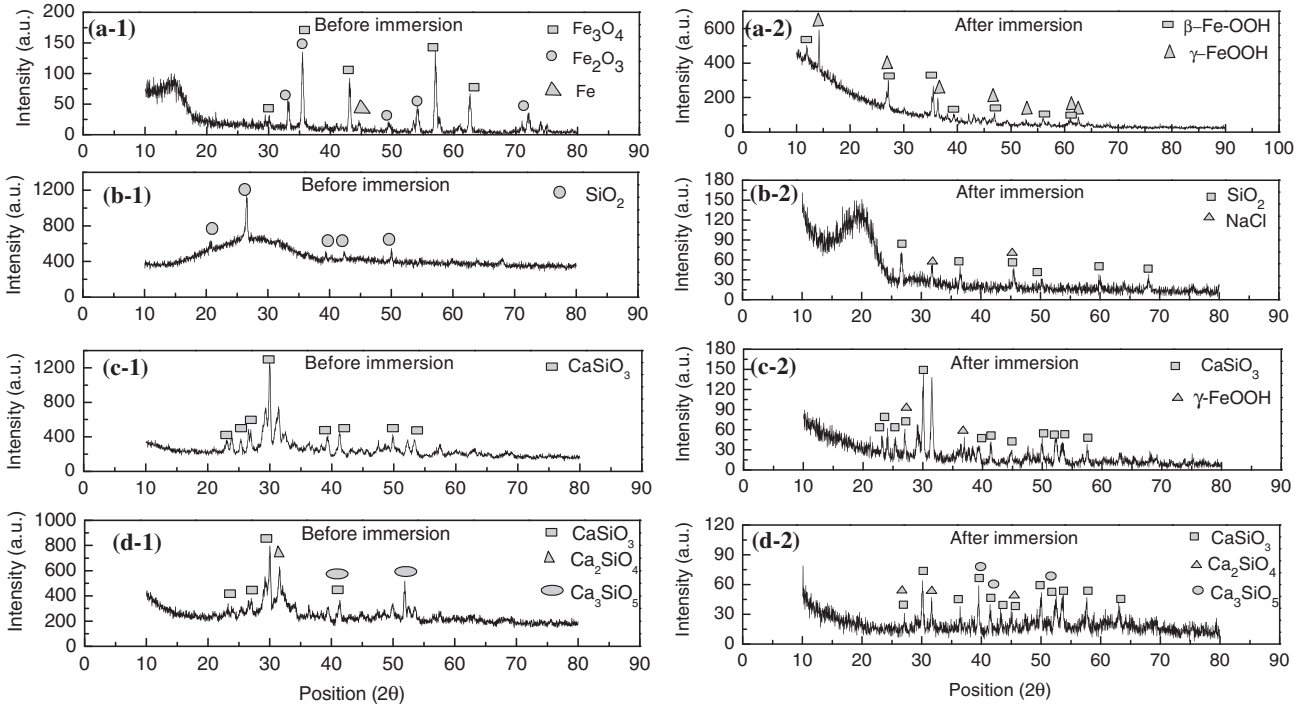

Fig. 4. XRD patterns on the surface of steel rebar before and after immersion tests in 3.5 wt.% NaCl solution: (a-1, a-2) uncoated rebar, (b-1, b-2) pure enamel coated rebar, (c-1, c-2) mixed enamel coated rebar, and (d-1, d-2) double enamel coated rebar.

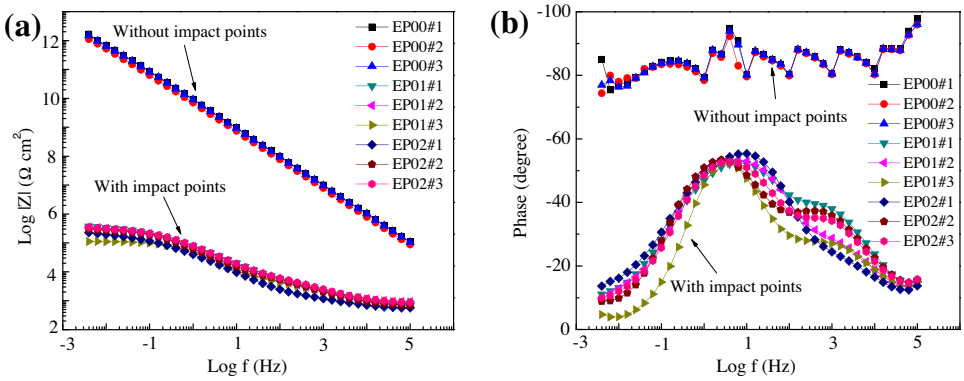

Fig. 5. EIS test results of FBE coated steel rebar in Bode format: (a) modulus, and (b) phase angle.

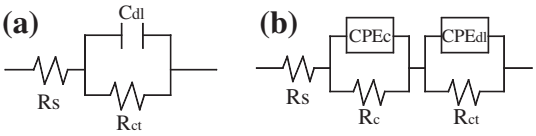

Fig. 6. EEC model for FBE coated rebar: (a) without impact points, and (b) with impact points.

the EIS test data. The Chi-squared value in the order of 10^{-3} confirmed a satisfactory fitting process.

Fig. 7a, b presents the effect of coating damage on the charge transfer resistance and the double layer capacitance of FBE coating, respectively. Each point represents the average of three samples with an error bar representing one standard deviation. It can be seen from Fig. 7 that all parameters vary little except for the exponent n_{dl} of damaged coating with 6 impact points. They indicated a high degree of consistency of FBE coating. For the FBE coating without impact points, a low double layer capacitance of 10^{-3} nF/cm^2 and a high charge transfer resistance of 10^6 MΩ cm^2 indicated a high degree of corrosion protection. For the FBE coating with impact points, the double layer capacitance increased to 10 μF/cm^2 and the charge transfer resistance decreased to 0.1 MΩ cm^2, corresponding to a significantly reduced degree of corrosion protection. The significant change in corrosion performance is attributed to the increased conductivity and capacitance as a result of chloride ions penetration through the impact-induced damage area. The numbers of impact points seemed to have little influence on the coating capacitance and charge transfer resistance. Fig. 7c shows a reduction of the exponent n_{dl} of CPE$_{dl}$ from 1.0 for the intact coating to 0.7 for damaged coating, indicating a significant drift of the electrochemical behavior away from a capacitor. This is because the impact-induced damage increased the non-homogeneity of FBE coating. Therefore, FBE coating is very sensitive to the onset of any damage.

3.3.2. Enamel coated steel bar

The electrochemical impedance spectra of uncoated and three types of enamel coated samples are presented in Fig. 8 in the format of Bode plots. It can be observed that all the plots featured two capacitive loops, similar to those for damaged FBE coating as shown in Fig. 5. Therefore, the EEC model in Fig. 6b was used to fit the EIS test results of uncoated and enamel coated rebar samples with or without impact points. In this model, R_c and CPE$_c$ respectively denote the resistance and capacitance of mill scale or enamel coatings. The Chi-squared value in the fitting process to EEC model was in the range between 10^{-4} and 10^{-3}.

The similarity between Fig. 8 and Fig. 5 for damaged FBE coating is attributed to the fact that enamel coatings have porous microstructures as illustrated in Fig. 3, non-uniform coating thickness due to the influence of rebar ribs, and potential coating defects induced during handling [29]. In particular, the impedance of the ME coating is nearly independent of the number of impact points as shown in Fig. 8c. For the PE and DE coatings, a greater number of impact points leads to smaller impedances, as shown in Fig. 8b, d.

Fig. 9 compares the properties of the uncoated and enamel coated rebar samples without impact points in terms of coating resistance R_c, coating capacitance C_c, and CPE$_c$ exponent n_c. In general, coating resistance and coating capacitance represent a degree of ability of coating to resist the penetration of electrolyte solution and the diffusion process of electrolyte solution into the coating, respectively [29,30]. Among the three enamel coatings as shown in Fig. 9, the PE coating had the lowest capacitance (0.2 μF/cm^2) and the highest resistance (1.3 kΩ cm^2). These values

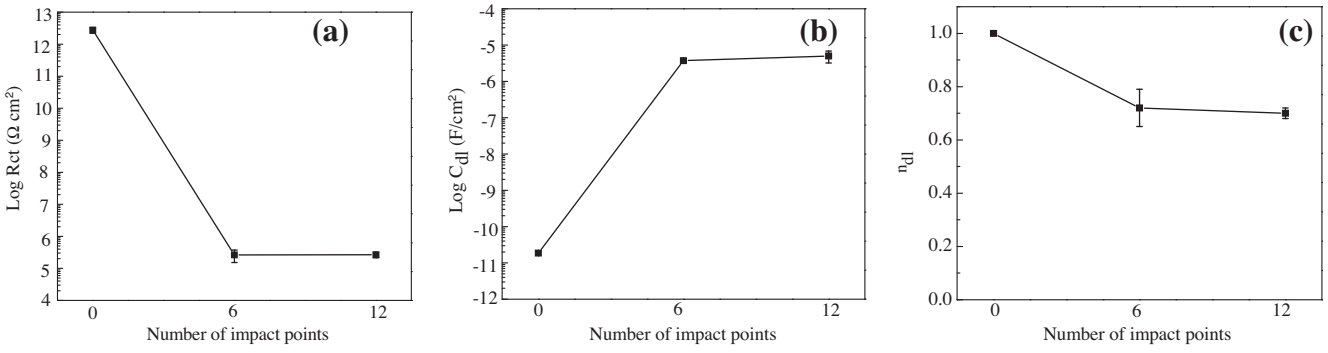

Fig. 7. Fitted parameters of FBE coated rebar: (a) charge transfer resistance R_{ct}, (b) double layer capacitance C_{dl}, and (c) CPE$_{dl}$ exponent n_{dl}.

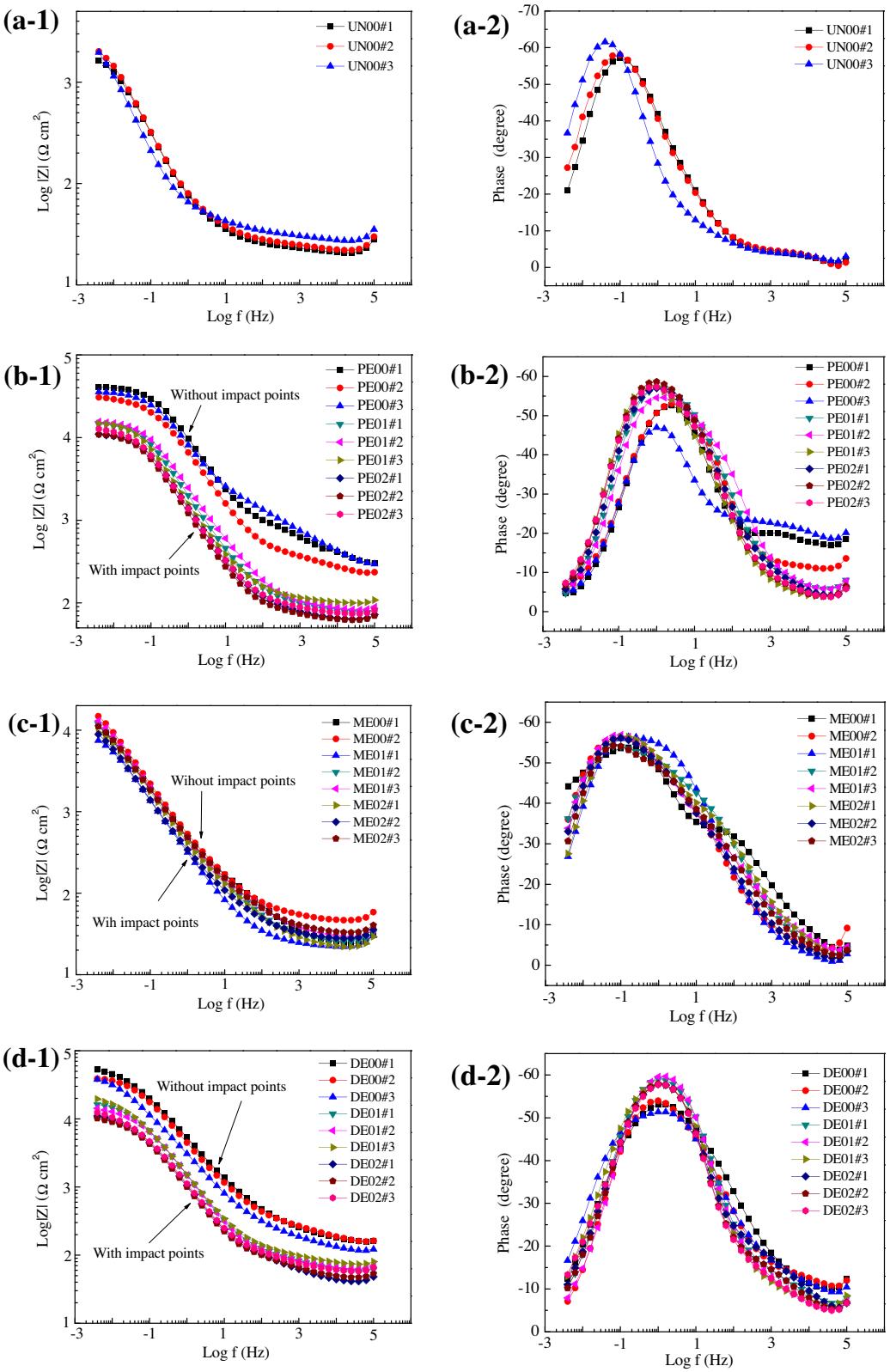

Fig. 8. EIS test results in Bode format for: (a-1, a-2) uncoated rebar, (b-1, b-2) pure enamel coated rebar, (c-1, c-2) mixed enamel coated rebar, and (d-1, d-2) double enamel coated rebar.

indicate the best protection of PE coating against chloride ion penetration, which is likely attributed to its less porous microstructure with isolated pores, as shown in Fig. 3b-1. On the other hand, the ME coating had the highest capacitance and relatively low resistance, indicating the least degree of prevention to chloride ion penetration. This is attributed to its more porous microstructure, with interconnected pores, as shown in Fig. 3d-1. The properties of the DE coating lie in between those of the PE and ME coatings. Compared to the uncoated rebar samples, however, all three enamel coatings had more favorable corrosion-protection properties than

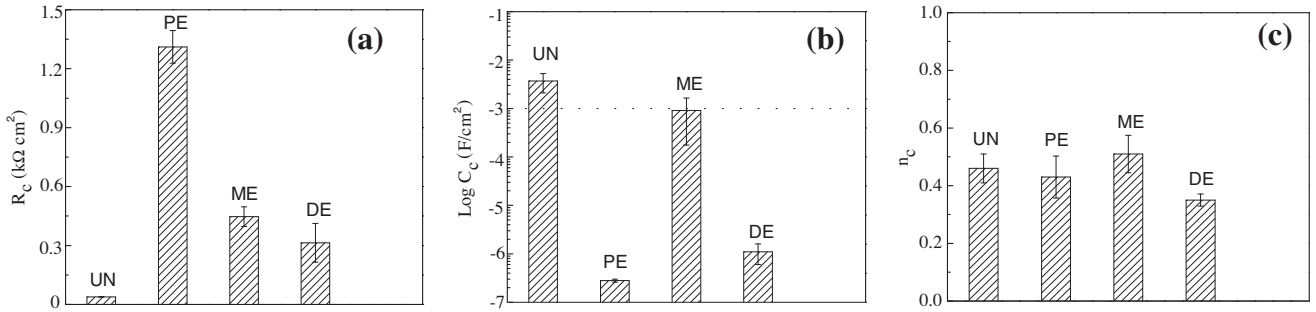

Fig. 9. Property of intact enamel coatings and mill scale: (a) coating resistance R_c, (b) coating capacitance C_c, and (c) CPE$_c$ exponent n_c.

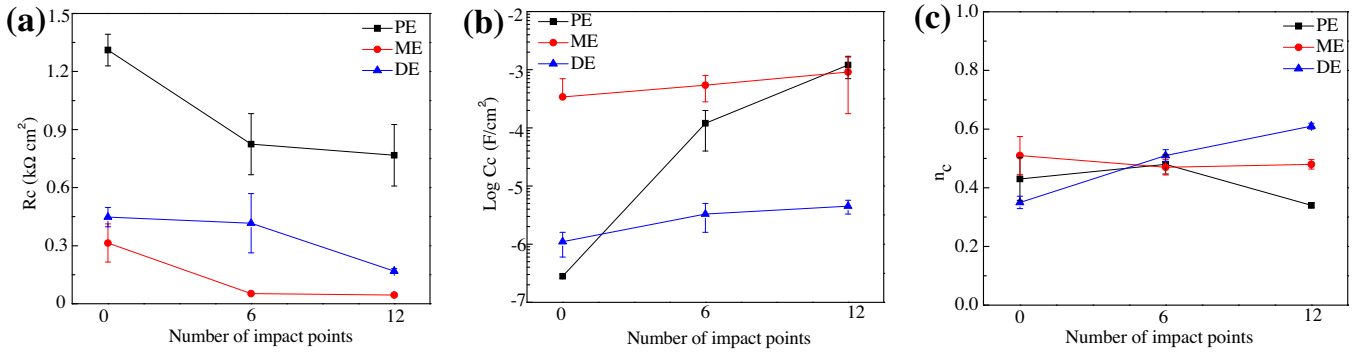

Fig. 10. Sensitivity of coating properties to impact points: (a) coating resistance R_c, (b) coating capacitance C_c, and (c) CPE$_c$ exponent n_c.

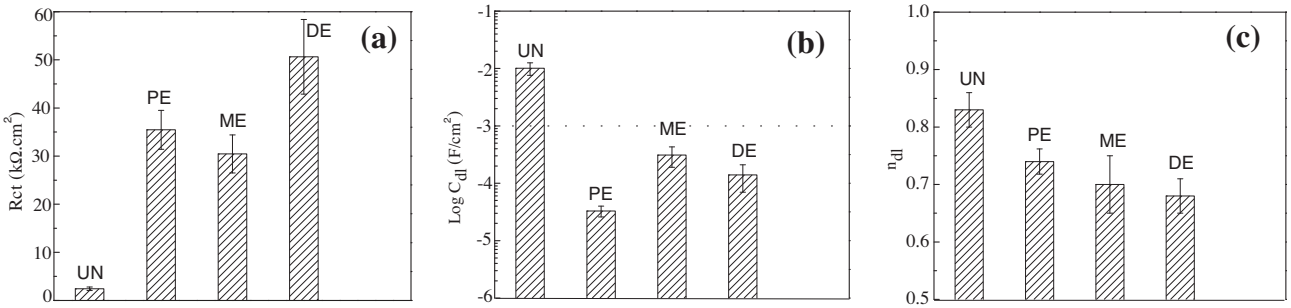

Fig. 11. Corrosion behavior of three enamel coated samples versus uncoated samples: (a) charge transfer resistance R_{ct}, (b) double layer capacitance C_{dl}, and (c) CPE$_{dl}$ exponent n_{dl}.

the mill scale on the surface of uncoated rebar. The exponent n_c varied from 0.4 to 0.5 for all the uncoated and enamel coated samples, indicating significant non-homogeneities that came from the non-uniform structure of mill scale and the non-uniform coating thickness and defect during handling for the uncoated and enamel coated rebar, respectively.

Fig. 10 shows the sensitivity of three types of enamel coatings to impact points in terms of coating resistance R_c, coating capacitance C_c, and CPE$_c$ exponent n_c. For all three enamel coatings, more impact points resulted in increasing capacitance and decreasing resistance to various extents. The PE and DE coatings were more sensitive to the number of impact points than the ME coating since the intact ME coating already revealed numerous interconnected pores and adding several impact points did not significantly increase the number of chloride ion penetration pathways. On the contrary, the intact PE and DE coatings had better barrier properties with isolated pores. Adding the damage points provided new pathways for chloride ions to penetrate through the coatings. As shown in Fig. 10c, the number of damage points did not affect significantly the electrochemical non-uniformity of all three enamel coatings.

Fig. 11 compares the corrosion resistance of uncoated rebar and enamel coated rebar samples without impact points in terms of charge transfer resistance, R_{ct}, and double layer capacitance, C_{dl}, and CPE$_{dl}$ exponent n_{dl}. The charge transfer resistance is inversely proportional to corrosion rate and is a measure of resistance to the transfer of electrons across the metal surface [31,32]. The double layer capacitance, calculated from Eq. (1), is a measure of ease of charge transfer. As shown in Fig. 11, in comparison with the ME coating, the DE and PE coatings had a relatively higher charge transfer resistance and lower double layer capacitance, which is indicative of a smaller exposed area of steel to the electrolyte solution. The uncoated rebar samples had the lowest charge transfer resistance and the highest double layer capacitance compared with

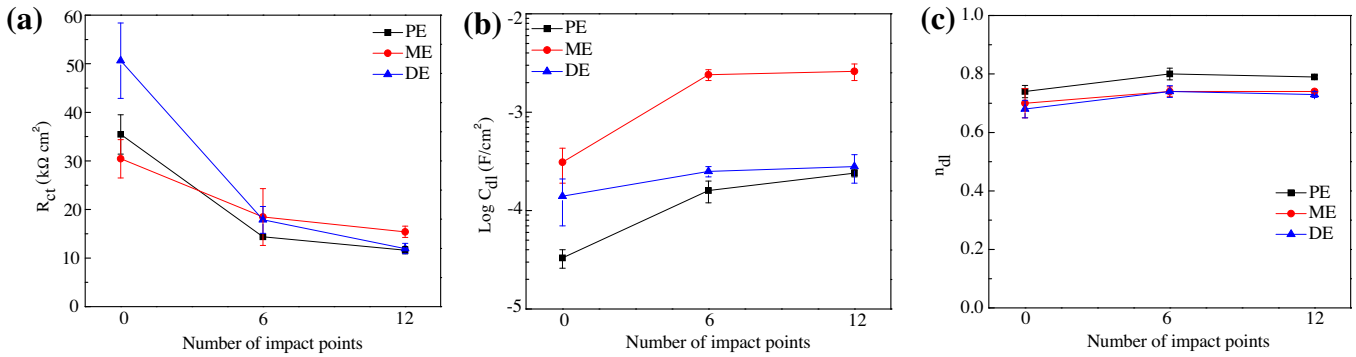

Fig. 12. Sensitivity of corrosion behavior of enamel coated samples to impact points: (a) charge transfer resistance R_{ct}, (b) double layer capacitance C_{dl}, and (c) CPE_{dl} exponent n_{dl}.

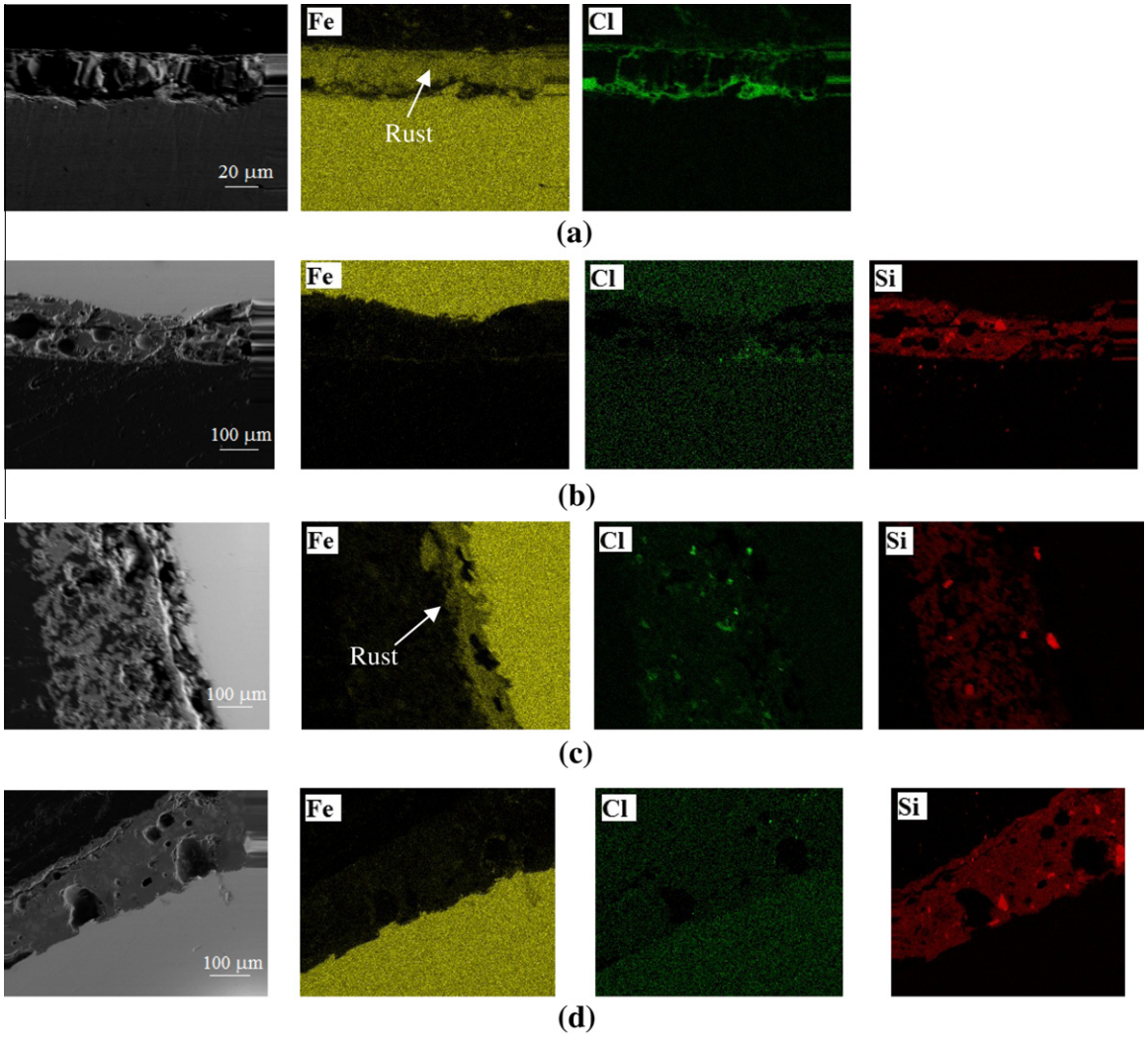

Fig. 13. Elemental distribution maps of electrochemical tested samples: (a) uncoated rebar, (b) pure enamel coated rebar, (c) mixed enamel coated rebar, and (d) double enamel coated rebar.

the three types of enamel coated samples. The CPE_{dl} exponents ranged from 0.65 to 0.85, indicating great non-homogeneities of both the uncoated and enamel coated samples.

Like Fig. 10 for coating property sensitivity to damage, Fig. 12 shows the corrosion sensitivity to impact points. Impact points increased the double layer capacitance and decreased the charge transfer resistance for all three types of enamel coatings. No significant difference was observed between the effect of 6 impact points and 12 impact points. As shown in Fig. 12c, there seems no obvious influence of impact-induced damage on the non-homogeneity of enamel coatings.

Compared with the FBE coating as shown in Fig. 7, all three enamel coatings, shown in Fig. 12, are significantly less sensitive to minor damage (0–6 points) but equally or more sensitive to further

damage (6–12 points). This can be explained as follows. Intact enamel coating had some regions of exposed steel that developed during handling; thus, additional minor damage of the coating did not significantly affect corrosion performance of the intact coating; and further coating damage contributed relatively less corrosion degradation. On the other hand, intact FBE coating was an effective corrosion barrier; thus minor damage of the FBE coating added new pathways for chloride ions penetration and significantly degraded corrosion performance, compared to the intact coating. Once initiated under minor damage, corrosion was extended rapidly underneath the FBE coating, which is typically referred to as under-film corrosion and will be further discussed in Section 3.5. In fact, the charge transfer resistance of the enamel coatings with impact points in Fig. 12a is in the same order of magnitudes as that for the damaged FBE coating, Fig. 7a.

3.4. Chloride diffusion through enamel coatings

Fig. 13 shows the cross-sectional elemental analysis of uncoated and enamel coated rebar samples after corrosion tests. For enamel coated rebar, the cross-sections were taken from the undamaged coating areas. For each sample, a SEM image and the corresponding distribution mappings for Fe, Cl, and Si were presented. Fe mapping was used for corrosion detection, Cl mapping was used for the detection of chloride ions, and Si mapping was used for the identification of the enamel coating location and thickness.

It can be observed from Fig. 13a, c that chloride ions were clearly detected in the rust layer of the uncoated rebar (as-received condition) and in the ME coating, revealing the diffusion of chloride ions through the mill scale and the ME coating. This is further verified by the corrosion product (rust) on the surface of the uncoated rebar and near the interface of the ME coating and its substrate steel. Corrosion products were concentrated near the interface mainly because the sample was immersed in salt solution for a short duration and corrosion products diffused through a part of the coating layer only. As shown in Fig. 13b, d, no chloride ions were detected inside the PE and DE coatings even though isolated pores were present as discussed previously. The Fe mappings also verified that little or no corrosion product was detected at the interface between the PE/DE coating and its substrate steel. Therefore, the PE and DE coatings are effective physical barriers that successfully prevented chloride ions from penetration.

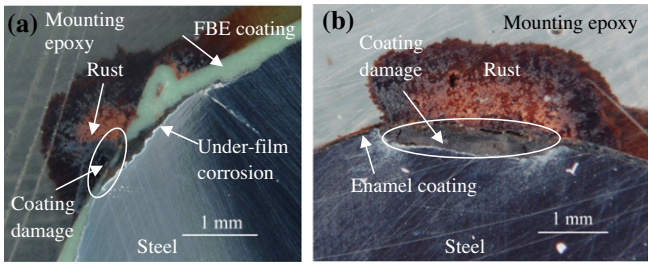

Fig. 15. Supporting evidences of corrosion mechanisms: (a) damaged FBE coating, and (b) damaged enamel coating.

3.5. Mechanism of the corrosion resistance of FBE coating and three enamel coatings

Based on the SEM images, electrochemical impedance spectra, and chloride distribution mappings, the corrosion mechanisms of the enamel coated steel in 3.5 wt.% NaCl solution can be summarized and illustrated as shown in Fig. 14b–d. They are compared with the corrosion mechanism of FBE coated rebar as illustrated in Fig. 14a. When it remains intact, the FBE coating is an effective physical barrier to protect the coated steel bar from corrosion. Once damaged, the FBE coating can no longer prevent the electrochemical reaction between the electrolyte and the steel, and its ability for corrosion protection is reduced dramatically. As illustrated in Fig. 14a, the damaged coating area provides a pathway for aggressive ions to penetrate through the coating layer and corrosion takes place on the surface of the exposed steel. Furthermore, once initiated, corrosion can extend beneath the coating, the so-called under-film corrosion as clearly illustrated in Fig. 15a. In recent years, such a corrosion mechanism for epoxy coated rebar was supported by several field studies in North America [33–35] where transportation and handling damage to FBE coatings is a culprit.

Similar to FBE coating, the intact PE and DE coatings as shown in Fig. 14b, d can also protect the coated steel rebar from corrosion, although the enamel coating with isolated air voids is not uniform, particularly around the rebar ribs. This non-uniformity makes the rib regions susceptible to corrosion attack. Due to its brittleness, enamel coatings are susceptible to impact damage. As a result, the enamel coated rebar often experiences corrosion pits at isolated damage locations as illustrated in Fig. 14b, d. Unlike the

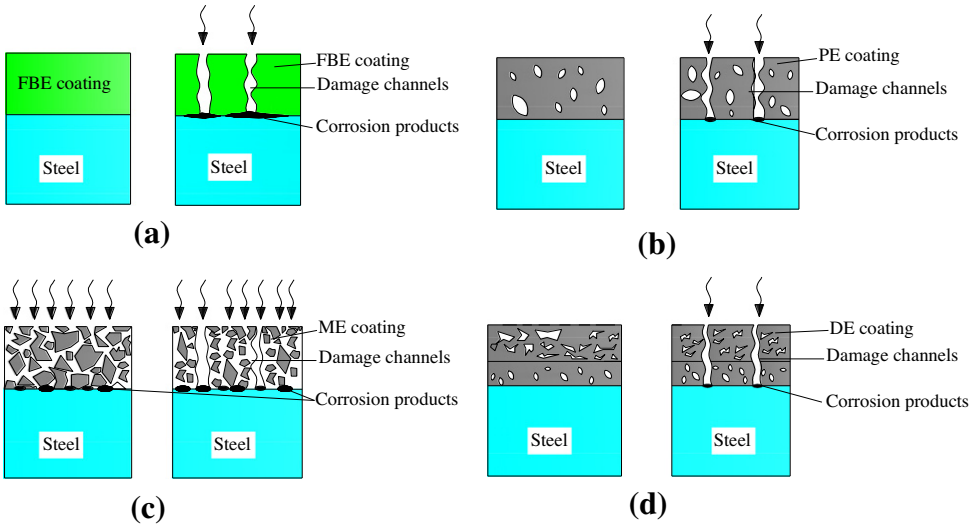

Fig. 14. Schemes of corrosion process of FBE and enamel coatings: (a) FBE coating (intact & damaged), (b) pure enamel coating (intact & damaged), (c) mixed enamel coating (intact & damaged), and (d) double enamel coating (intact & damaged).

FBE coating, enamel coating is chemically bonded to its steel substrate [36], limiting the pitted corrosion in the vicinity of the damaged coating area, avoiding the under-film corrosion in the enamel coated rebar as detailed in Fig. 15b.

As shown in Fig. 14c, the corrosion mechanism of the ME coating differs from those of the PE and DE coatings. Even for an undamaged coated rebar, the ME coating has interconnected pores due to the addition of Ca-silicate particles, potentially providing multiple pathways for aggressive ions to penetrate and resulting in widespread corrosion along the length of coated rebar. Therefore, corrosion in the ME coating takes place early on and is insensitive to additional damage that may be caused during transportation and handling.

4. Conclusions

In this study, the corrosion resistances of pure, mixed, and double enamel coatings applied on reinforcing steel bars were evaluated by means of electrochemical impedance spectroscopy. Their performance was compared with commercially available FBE coating. Corrosion sensitivity to coating damage was investigated with controlled levels of damage induced by a standard impact tester. Based on the test results, the following conclusions can be drawn about the corrosion performance of these coated samples:

(1) The intact double and pure enamel coatings provided a much higher degree of corrosion protection than the mixed enamel coating with 50% calcium silicate by weight mainly due to the absence of interconnected pores in the double and pure enamel coatings. All enamel coatings were significantly outperformed by the intact FBE coating.
(2) The corrosion performances of the double and pure enamel coatings were more sensitive to damage than the mixed enamel coatings because damage provides corrosion pathways that did not exist in the undamaged DE and PE samples. The corrosion resistance of FBE coating was most sensitive to damage and, once damaged, was in the same order of that for the damaged enamel coatings.
(3) Pitted corrosion of both double and pure enamel coatings was initiated at the location of damaged coating areas but restrained locally due to well-adhered glassy layers on the surface of coated rebar. Interconnected regions of calcium silicate particles in the mixed enamel coating appeared to provide a corrosion pathway to the underlying steel rebar so that both uniform and pitted corrosions occurred on the surface of damaged coated rebar. Although superior when undamaged, the corrosion performance of the FBE coating significantly degraded with local damage of the sort that can occur during transportation and handling due to the well-known under-film corrosion mechanism.
(4) The non-uniformity of coating thickness due to rebar deformation must be overcome with an alternative enameling process to improve the corrosion performance of enamel coatings for practical applications.

Acknowledgement

The authors gratefully acknowledge the financial support provided by the US National Science Foundation under Award No. CMMI-0900159, by the Missouri Department of Transportation under Award No. 28015485-09R000587, and by the Center for Transportation Infrastructure and Safety at Missouri University of Science and Technology under Award No. DTRT06-G-0014. The enamel-coated specimens tested in this study were prepared by Pro-Perma Engineered Coatings, Rolla, Missouri. The authors would also like to thank continuing support and assistance received from the research team members, including Drs. Signo Reis and Dongming Yan, Chenglin Wu, and Xiaoming Cheng. Special thanks are due to Professor Kent Peaslee from the Department of Materials Science and Engineering at Missouri University of Science and Technology for his assistance in steel composition analysis.

References

[1] G.H. Koch, M.P.H. Brongers, N.G. Thompson, Y.P. Virmani, J.H. Payer, Corrosion costs and preventive strategies in the United States, Publication No. FHWA-RD-01-156, NACE International, Houston TX, USA, 2002.
[2] J.P. Broomfield, Corrosion of steel in concrete: understanding, investigation and repair, 2nd edition., Taylor & Francis, New York, 2007.
[3] D.A. Jones, Principles and prevention of corrosion, 2nd edition., Prentice Hall, New Jersey, 1996.
[4] A. Conde, J.J. de Damborenea, Electrochemical impedance spectroscopy for studying the degradation of enamel coatings, Corros. Sci. 44 (2002) 1555–1567.
[5] A. Conde, J.J. de Damborenea, Monitoring of vitreous enamel degradation by electrochemical noise, Surf. Coat. Technol. 150 (2002) 212–217.
[6] V.F. Hock, S.W. Morefield, D.C. Day, C.A. Weiss, Jr., P.G. Malone, The use of vitreous enamel coatings to improve bonding and reduce corrosion in concrete reinforcing steel, NACE International, CORROSION 2008, March 16–20, 2008, New Orleans LA, Paper No. 08220.
[7] C.L. Hackler, C.A. Weiss, P.G. Malone, Reactive porcelain enamel coatings for reinforcing steel to enhance the bond to concrete and reduce corrosion, XXI International Enamellers Congress, May 18–22, 2008, Shanghai, China. pp. 11–18.
[8] V.F. Hock, S.W. Morefield, C.A. Weiss Jr., P.G. Malone, The use of vitreous enamel coatings to improve bonding and reducing corrosion in concrete reinforcing steel and stay-in-place forms at army installations, Department of Defense Corrosion Conference, Gaylord National, Washington DC, 2009.
[9] K.M. Fyles, P. Shorrock, Alkali resistant glass fibers for cement reinforcement, US Patent 4345,037, Pilkington Brothers Ltd. (GB), 1982.
[10] NRC, International critical tables, vol. 2, National Research Council(NRC), McGraw-Hill, Washington, DC, 1927, p. 116.
[11] ASTM, Standard specification for Portland cement, American Society of Testing Methods (ASTM), C150-07, 2007.
[12] ASTM, Standard Test Method for Impact Resistance of Pipeline Coatings (Falling Weight Test), American Society of Testing Methods (ASTM), G14-04, 2010.
[13] T.D. Marcotte, Characterization of chloride-induced corrosion products that form in steel-reinforced cementitious materials, Ph.D. Dissertation, University of Waterloo, Canada, 2001.
[14] P.A. Schweitzer, Corrosion and corrosion protection handbook, 2nd edition., CRC Press, New York, 1989.
[15] J.K. Singh, D.D.N. Singh, The nature of rusts and corrosion characteristics of low alloy and plain carbon steel in three kinds of concrete pore solution with salinity and different pH, Corros. Sci. 56 (2012) 129–142.
[16] Y. Zhao, H. Ren, H. Dai, W. Jin, Composition and expansion coefficient of rust based on X-ray diffraction and thermal analysis, Corros. Sci. 53 (2011) 1646–1658.
[17] Y. Ma, Y. Li, F. Wang, Corrosion of low carbon steel in atmospheric environments of different chloride content, Corros. Sci. 51 (2009) 997–1006.
[18] C.G. Oliveira, M.G.S. Ferreira, Ranking high-quality paint systems using EIS. Part I: intact coatings, Corros. Sci. 45 (2003) 123–138.
[19] C.G. Oliveira, M.G.S. Ferreira, Ranking high-quality paint systems using EIS. Part II: defective coatings, Corros. Sci. 45 (2003) 139–147.
[20] X. Shi, T.A. Nguyen, Z. Suo, Y. Liu, R. Avci, Effect of nanoparticles on the anticorrosion and mechanical properties of epoxy coating, Surf. Coat. Technol. 204 (2009) 237–245.
[21] Y. Huang, H. Shi, H. Huang, J. Daugherty, S. Wu, S. Ramanathan, C. Chang, Florian Mansfeld, Evaluation of the corrosion resistance of anodized aluminum 6061 using electrochemical impedance spectroscopy (EIS), Corros. Sci. (2008) 3569–3575.
[22] W. Aperador, R. Mejia de Gutierrez, D.M. Bastidas, Steel corrosion behavior in carbonated alkali-activated slag concrete, Corros. Sci. 51 (2009) 2027–2033.
[23] Y.S. Choi, J.G. Kim, K.M. Lee, Corrosion behavior of steel rebar embedded in fly ash concrete, Corros. Sci. 48 (2006) 1733–1745.
[24] M.G. Maitra, M. Sinha, A.K. Mukhopadhyay, T.R. Middya, U. De, S. Tarafdar, Ion-conductivity and Young's modulus of the polymer electrolyte PEO-ammonium perchlorate, Solid State Ionics 178 (2007) 167–171.
[25] Y. Zhang, Y. Huang, L. Wang, Study of EVOH based single ion polymer electrolyte: composition and microstructure effects on the proton conductivity, Solid State Ionics 177 (2006) 65–71.
[26] M.J. Rodiguez Presa, R.I. Tucceri, M.I. Florit, D. Posada, Constant phase element behavior in the poly (o-toluidine) impedance response, J. Electroanal. Chem. 502 (2001) 82–90.
[27] Z. Yao, Z. Jiang, F. Wang, Study on corrosion resistance and roughness of micro-plasma oxidation ceramic coatings on Ti alloy by EIS technique, Electrochim. Acta 52 (2007) 4539–4546.
[28] M. Mahdavian, R. Naderi, Corrosion inhibition of mild steel in sodium chloride solution by some zinc complexes, Corros. Sci. 53 (2011) 1194–1200.

[29] C.R. Werner, Corrosion resistance of enamel-coated steel reinforcement for concrete, MS Thesis, Missouri University of Science and Technology, USA, 2010.
[30] Y. Zhang, Y. Shao, T. Zhang, G. Meng, F. Wang, The effect of epoxy coating containing emeraldine base and hydrofluoric acid doped polyaniline on the corrosion protection of AZ91D magnesium alloy, Corros. Sci. 53 (2011) 3747–3755.
[31] X.W. Liu, J.P. Xiong, Y.W. Lv, Y. Zuo, Study on corrosion electrochemical behavior of several different coating systems by EIS, Prog. Org. Coat. 64 (2009) 497–503.
[32] H.H. Hassan, E. Abdelghani, M.A. Amin, Inhibition of mild steel corrosion in hydrochloric acid solution by triazole derivatives: Part I. polarization and EIS studies, Electrochim. Acta 52 (2007) 6359–6366.
[33] D.G. Manning, Corrosion performance of epoxy-coated reinforcing steel: North American experience, Constr. Build. Mater. 10 (1996) 349–365.
[34] A. Zayed, A. Sagues, R. Powers, Corrosion of epoxy-coated reinforcing steel, Paper No. 379, NACE International, Houston TX, USA, 1989.
[35] L.L. Smith, R.J. Kessler, R.G. Powers, Corrosion of epoxy-coated rebar in a marine environment, Transportation Research Circular: Epoxy-Coated Reinforcement in Highway Structures, No. 403. National Research Council, Transportation Research Board, Washington, 1993, pp. 36–45.
[36] D.M. Yan, S. Reis, X. Tao, G.D. Chen, R.K. Brow, M.L. Koenigstein, Effect of chemically reactive enamel coating on bonding strength at steel/mortar interface, Constr. Build. Mater. 28 (2012) 512–518.